



Novel anisotropic elastoplastic modeling of K₀-consolidated sands

Journal:	<i>Canadian Geotechnical Journal</i>
Manuscript ID	cgj-2025-0539.R1
Manuscript Type:	Research Article
Date Submitted by the Author:	20-Nov-2025
Complete List of Authors:	Li, Jian; Beijing Jiaotong University Yin, Zhen-Yu; Hong Kong Polytechnic University, Department of Civil and Environmental Engineering
Is the manuscript for consideration in a Special Issue or Collection?:	Not applicable (regular submission)
Keyword:	Sand, Yield function, Anisotropy, K ₀ -consolidaiton, Constitutive model

SCHOLARONE™
Manuscripts

Novel anisotropic elastoplastic modeling of K_0 -consolidated sands

Jian LI and Zhen-Yu YIN

Jian LI, Associate Professor

Key Laboratory of Urban Underground Engineering of Ministry of Education, Beijing Jiaotong University, Beijing 100044, China; School of Civil Engineering, Beijing Jiaotong University, Beijing 100044, China. Email: jianli@bjtu.edu.cn

Zhen-Yu YIN, Professor (corresponding author)

Department of Civil and Environmental Engineering, The Hong Kong Polytechnic University, Hung Hom, Kowloon, Hong Kong. Tel: +852 3400 8470; Fax: +852 2334 6389; Email: zhenyu.yin@polyu.edu.hk

Draft

Abstract:

Accurately defining the yield surface is a cornerstone of constitutive modeling for sands, as it governs the onset and evolution of plastic deformation under various stress paths. This study proposes and compares some new anisotropic yield functions for K_0 -consolidated sands by introducing two shape parameters (n and χ) and one anisotropic state variable (α). For the proposed yield surfaces, the elastoplastic constitutive model is developed within a bounding surface plasticity framework, using a simplified form of the yield function as the plastic potential. Both inherent and induced anisotropy are captured through kinematic hardening and rotational evolution mechanisms. The performance of the proposed yield surfaces is evaluated through two complementary studies. First, the effects of degradation in n , χ and α on model performance are systematically investigated. Second, a parameter sensitivity analysis is conducted to assess the influence of key model parameters. Results show that with increasing anisotropic consolidation, the proposed model, characterized by flexible shape control and anisotropic state representation, achieves significantly improved predictive accuracy compared to existing models.

Keywords: Sand; Yield function; Anisotropy; K_0 -consolidation; Constitutive model

1. Introduction

The formulation of an appropriate yield surface is a fundamental aspect of constitutive modeling for sands. Common yield surface types used in sand models include the linear yield surface (Poorooshasb et al. 1966, 1967; Dubujet and Doanh 1997; Li and Dafalias 2000; Yang and Li 2004), the double yield surface (Liang et al. 1991; Yin et al. 2016), and the droplet-shaped yield surface (Yu 1998; Yao et al. 2004, 2019), all typically defined in the mean effective stress and deviatoric stress ($p' - q$) plane. The linear yield surface starts from the origin and reflects a linear relationship between deviatoric stress and mean effective stress. When combined with a non-associative flow rule, it has been used to simulate both dilative and contractive behaviors of sand. However, due to its open form, the linear yield surface cannot capture yielding during consolidation under constant stress ratios when the stress ratio is below the critical state value. To address this limitation, the double yield surface has been introduced, which incorporates a cap yield surface intersecting the mean effective stress axis to better describe consolidation behavior under constant stress ratios. In the model proposed by Liang et al. (1991), a parabolic surface is adopted in place of the linear component. Additionally, the droplet-shaped yield surface has been widely employed in unified models for both clays and sands; under specific values of the shape parameter, it simplifies to the elliptical yield surface of the modified Cam-Clay model (Roscoe and Burland 1968).

For constitutive models that account for the anisotropic behavior of K_0 -consolidated sands, several types of inclined yield surfaces have been developed. These include the inclined open narrow wedge surface (Liu et al. 2019; Pan and Rotta Loria 2024), the inclined

closed narrow wedge surface (Taiebat and Dafalias 2008; Landivar Macias and Rotta Loria 2023), the inclined elliptical surface (Asaoka et al. 2002; Zhang et al. 2007, 2011), and the inclined distorted lemniscate surface (Pestana and Whittle 1999). These models typically utilize anisotropic tensors or back-stress ratio tensors to characterize material anisotropy. Similar to the linear yield surface, the inclined open wedge surface fails to capture yielding during consolidation under constant stress ratios. On the other hand, both the inclined elliptical and distorted lemniscate yield surfaces have been incorporated into unified anisotropic models for clays and sands. Under certain parameter values, these yield surfaces degenerate to those of the original or modified Cam-Clay models (Roscoe et al. 1963; Roscoe and Burland 1968).

Notably, the MIT-S1 model proposed by Pestana and Whittle (1999) conducted numerical simulations of triaxial compression and extension tests on K_0 -consolidated sands. However, the predictive performance of the yield surface and the overall model remains unverified, as no direct comparisons with experimental data were presented. Despite these developments, none of the aforementioned anisotropic yield surfaces for sands have been rigorously validated against both triaxial compression and extension tests under K_0 -consolidated conditions. In particular, predictive validation under triaxial extension loading remains notably insufficient.

To overcome the limitations of conventional yield surfaces in representing the anisotropic response of K_0 -consolidated sands, this study extends a previously developed anisotropic yield function, originally proposed for clays, to sands. The proposed approach

introduces enhanced flexibility in yield surface geometry by incorporating two shape-controlling parameters (n and χ) and one evolving anisotropic state variable (α). A new elastoplastic constitutive model is developed on this basis and incorporated into a bounding surface plasticity framework. Particular emphasis is placed on evaluating the model's capability to capture the complex behavior of very loose K_0 -consolidated Hostun sand observed in undrained triaxial tests under both compression and extension conditions.

2. Anisotropic Yield Surface for K_0 -Consolidation Sand

2.1 Formulations of the Anisotropic Yield Surface for K_0 -Consolidated Sands and Parameter Analysis

Yin and Li (2025) proposed an anisotropic yield surface for K_0 -consolidated clays. Based on this yield function, an anisotropic elasto-plastic bounding surface model was developed, which demonstrated strong predictive capabilities by capturing the mechanical response of reconstituted K_0 -consolidated clays under both anisotropic consolidation and shear conditions, with good agreement observed between simulations and experimental results. The anisotropic yield function for K_0 -consolidated clays is expressed as follows:

$$f = \frac{M - \alpha}{nM + \alpha} \left[\frac{\frac{3}{2}(\mathbf{r} - \boldsymbol{\alpha}_d) : (\mathbf{r} - \boldsymbol{\alpha}_d)}{(M - \alpha)^2} \right]^{\frac{n+1}{2}} p' + p' - p_c \quad (1)$$

where $\mathbf{r} = \boldsymbol{\sigma}_d / p'$ is the stress ratio tensor; $\boldsymbol{\sigma}_d = \boldsymbol{\sigma}' - p'\boldsymbol{\delta}$ is the deviatoric stress tensor; $\boldsymbol{\delta}$ is the Kronecker delta; $\boldsymbol{\alpha}_d$ is the deviatoric fabric tensor (dimensionless and of the same form as $\boldsymbol{\sigma}_d$); parameter n control the shape of the yield surface, M is the slope of the critical state line in the $p'-q$ plane; q is deviatoric stress; p_c defines the size of the yield

surface. For a cross-anisotropic specimen, $\alpha = \sqrt{3/2(\boldsymbol{\alpha}_d : \boldsymbol{\alpha}_d)}$ represents the inclination of the yield ellipse.

Yao et al. (2004, 2019) proposed an approach to extend a yield surface originally formulated for clays to sandy soils by introducing a shape parameter χ . Incorporating this parameter, the Modified Cam-Clay (MCC) yield surface can be expressed in the following form:

$$f = \frac{(1 + \chi)^{\frac{3}{2}} \mathbf{r} : \mathbf{r}}{M^2 - \chi^{\frac{3}{2}} \mathbf{r} : \mathbf{r}} p' + p' - p_c \quad (2)$$

The parameter χ controls the geometry of the yield surface. When $\chi = 0$, the yield surface reduces to the elliptical form characteristic of the MCC model. For $\chi > 0$, the yield surface adopts a drop-like shape. Moreover, increasing χ leads to a flatter yield surface at elevated stress ratios ($\eta = q / p'$), which corresponds to a more pronounced strain-softening response.

Building upon the two yield surface formulations described above, namely the anisotropic yield surface for K_0 -consolidated clays proposed by Yin and Li (2025) and the shape-controlled yield surface for sands introduced by Yao et al. (2004, 2019), the present study extends the former to sands. Based on these two formulations, six possible combined yield surface forms are proposed as follows:

$$f_1 = \frac{M - \alpha}{nM + \alpha} \left[\frac{(1 + \chi)^{\frac{3}{2}} (\mathbf{r} - \boldsymbol{\alpha}_d) : (\mathbf{r} - \boldsymbol{\alpha}_d)}{(M - \alpha)^2 - \chi(\frac{3}{2} \mathbf{r} : \mathbf{r})} \right]^{\frac{n+1}{2}} p' + p' - p_c \quad (3)$$

$$f_2 = \frac{M - \alpha}{nM + \alpha} \left[\frac{(1 + \chi)^{\frac{3}{2}} (\mathbf{r} - \boldsymbol{\alpha}_d) : (\mathbf{r} - \boldsymbol{\alpha}_d)}{(M - \alpha)^2 - \chi(\frac{3}{2} \mathbf{r} : \mathbf{r} - \frac{3}{2} \boldsymbol{\alpha}_d : \boldsymbol{\alpha}_d)} \right]^{\frac{n+1}{2}} p' + p' - p_c \quad (4)$$

$$f_3 = \frac{M - \alpha}{nM + \alpha} \left[\frac{(1 + \chi) \frac{3}{2}(\mathbf{r} - \boldsymbol{\alpha}_d) : (\mathbf{r} - \boldsymbol{\alpha}_d)}{(M - \alpha)^2 - \chi \frac{3}{2}(\mathbf{r} - \boldsymbol{\alpha}_d) : (\mathbf{r} - \boldsymbol{\alpha}_d)} \right]^{\frac{n+1}{2}} p' + p' - p_c \quad (5)$$

$$f_4 = \frac{M - \alpha}{nM + \alpha} \left[\frac{\frac{3}{2}(\mathbf{r} - \boldsymbol{\alpha}_d) : (\mathbf{r} - \boldsymbol{\alpha}_d)}{(M - \alpha)^2 - \chi(\frac{3}{2}\mathbf{r} : \mathbf{r})} \right]^{\frac{n+1}{2}} p' + p' - p_c \quad (6)$$

$$f_5 = \frac{M - \alpha}{nM + \alpha} \left[\frac{\frac{3}{2}(\mathbf{r} - \boldsymbol{\alpha}_d) : (\mathbf{r} - \boldsymbol{\alpha}_d)}{(M - \alpha)^2 - \chi(\frac{3}{2}\mathbf{r} : \mathbf{r} - \frac{3}{2}\boldsymbol{\alpha}_d : \boldsymbol{\alpha}_d)} \right]^{\frac{n+1}{2}} p' + p' - p_c \quad (7)$$

$$f_6 = \frac{M - \alpha}{nM + \alpha} \left[\frac{\frac{3}{2}(\mathbf{r} - \boldsymbol{\alpha}_d) : (\mathbf{r} - \boldsymbol{\alpha}_d)}{(M - \alpha)^2 - \chi \frac{3}{2}(\mathbf{r} - \boldsymbol{\alpha}_d) : (\mathbf{r} - \boldsymbol{\alpha}_d)} \right]^{\frac{n+1}{2}} p' + p' - p_c \quad (8)$$

The six yield functions can be classified into two groups. In the first group, both the numerator and denominator of the first term contain the parameter χ , whereas in the second group, only the denominator of the first term includes χ . Furthermore, within each group, the differences among the three yield functions lie in the specific form of the parameter χ appearing in the denominator of the first term, which takes the form of $\chi(\frac{3}{2}\mathbf{r} : \mathbf{r})$, $\chi(\frac{3}{2}\mathbf{r} : \mathbf{r} - \frac{3}{2}\boldsymbol{\alpha}_d : \boldsymbol{\alpha}_d)$ and $\chi \frac{3}{2}(\mathbf{r} - \boldsymbol{\alpha}_d) : (\mathbf{r} - \boldsymbol{\alpha}_d)$, respectively.

To ensure the mathematical stability of the yield surface expression, the denominator of its first term must remain positive. However, when the yield surfaces are defined by Eqs. (3) and (6), the denominator in the first term may become negative under large values of the shape parameter χ and the stress ratio η , potentially leading to numerical instability. Therefore, greater emphasis is placed on the comparative analysis of the yield surfaces defined by Eqs. (4), (5), (7) and (8) in the subsequent sections.

Although both n and χ influence the shape of the yield surface, they affect it in distinct ways (see Fig. 1). As n increases, the right half of the yield surface expands while the left half contracts. The intersection of the upper part of the yield surface with the critical

state line in compression (CSLc) moves upward and rightward, whereas the intersection with the extension line (CSLe) remains relatively unchanged. When $n = 0.5$, the surface is very close to that of original Cam-Clay model (OCC) (Roscoe et al. 1963) but with improvement of the horizontal, rather than inclined, outer normal direction of the yield surface at the right intersection with the α line. When $n = 1$, the yield surface converges toward that of the MCC model (Roscoe and Burland 1968).

In contrast, increasing χ causes the yield surface to flatten, gradually forming a droplet shape. Its intersection with the critical state line shifts toward the origin, and ultimately coincides with it. It is important to note that, as the parameter χ increases, the right portion of the yield surface defined by Eq. (7) progressively expands beneath the α line—an evolutionary pattern that stands in stark contrast to those exhibited by the yield surfaces defined by the other three formulations.

Fig. 2 illustrates the shapes of the four yield surfaces defined by Eqs. (4), (5), (7) and (8) for different values of the shape parameter χ . When $\chi = 0.25$, the yield surface defined by Eq. (4) is slightly flatter above the α line but less flattened below it compared to that defined by Eq. (5). As χ increases to 1, the yield surface defined by Eq. (4) becomes overall less flattened than the one defined by Eq. (5). Compared to the yield surfaces defined by Eqs. (4) and (5), those defined by Eqs. (7) and (8) are generally less flattened under the same values of the shape parameter χ .

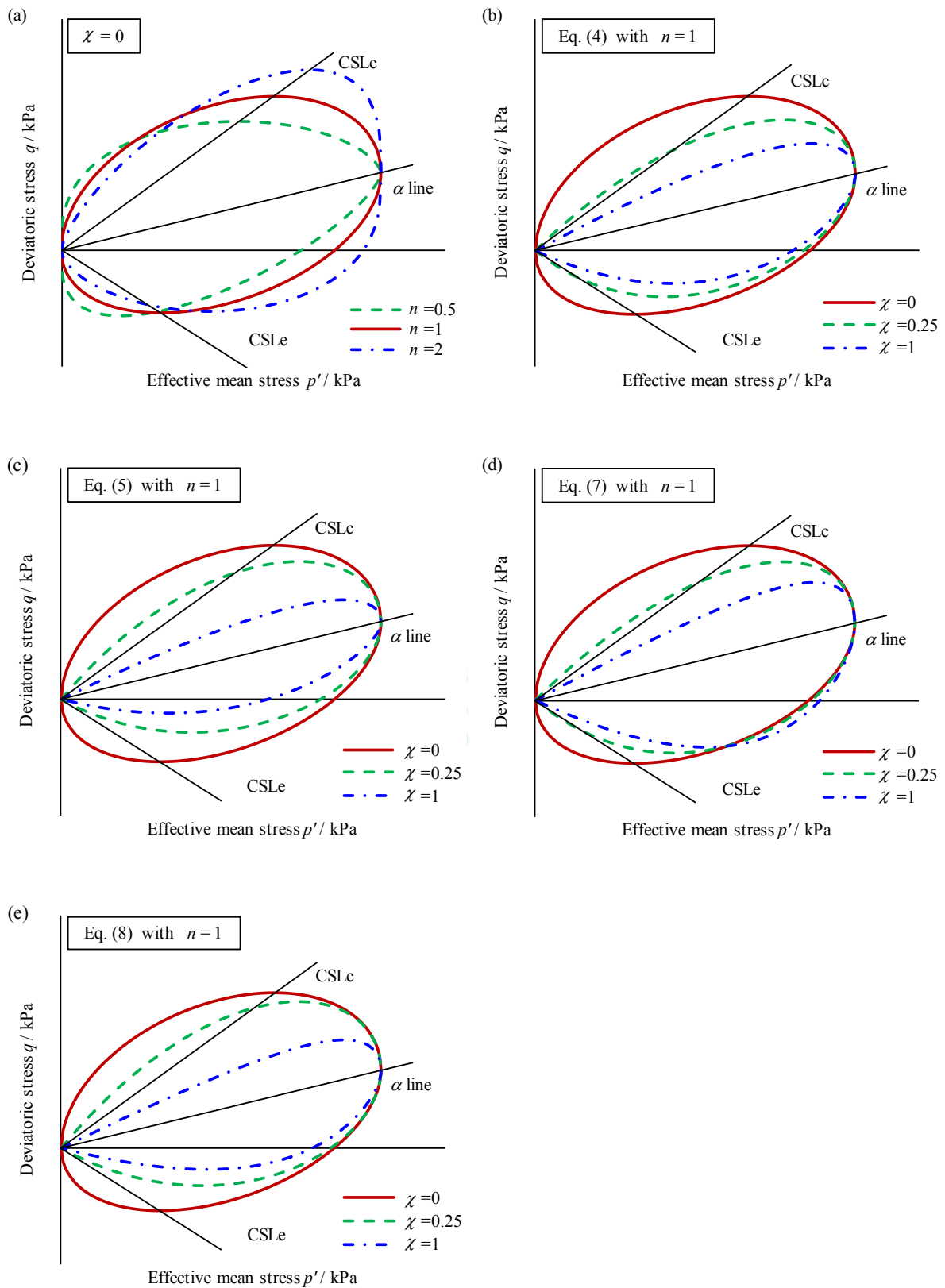


Fig. 1 Influence of parameters (a) n and (b)-(e) χ on the shape of the yield surface

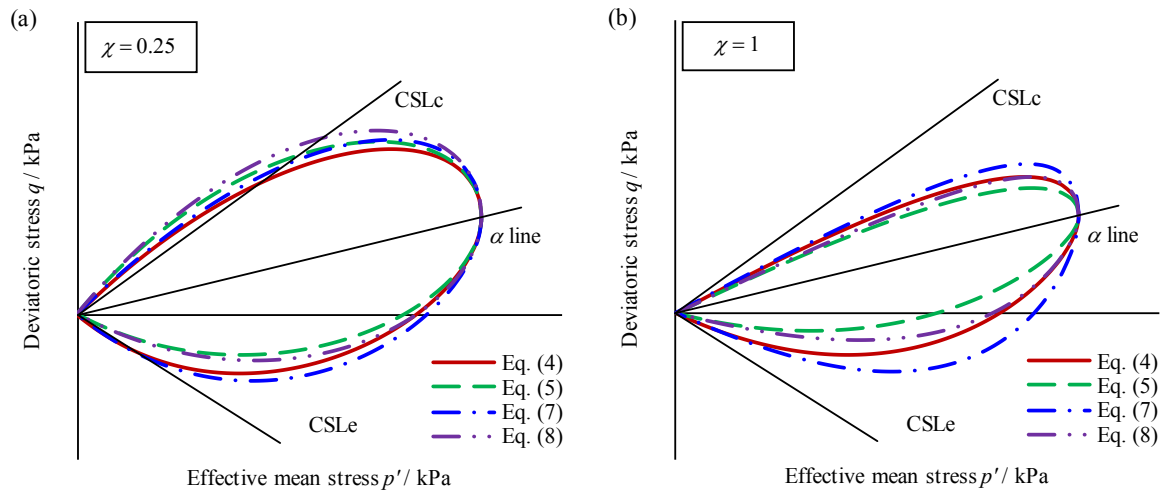


Fig. 2 The shapes of the four yield surfaces with (a) $\chi = 0.25$ and (b) $\chi = 1$

To properly model shear behavior in general stress space, the critical state line slope M is modified using the Lode angle-dependent function proposed by Sheng et al. (2000):

$$M = M_c \left[\frac{2c^4}{1 + c^4 + (1 - c^4) \sin 3\theta} \right]^{\frac{1}{4}} \quad (9)$$

$$\frac{-\pi}{6} \leq \theta = \frac{1}{3} \sin^{-1} \left(\frac{-3\sqrt{3}\bar{J}_3}{2\bar{J}_2^{3/2}} \right) \leq \frac{\pi}{6}, \quad \bar{J}_2 = \frac{1}{2} \bar{s} : \bar{s}, \quad \bar{J}_3 = |\bar{s}|, \quad \bar{s} = \sigma_d - p' \alpha_d \quad (10)$$

where $c = (3 - \sin \phi_c) / (3 + \sin \phi_c)$ according to Mohr-Coulomb yield criterion; ϕ_c is the internal friction angle; θ is the lode angle; η is stress ratio defined by q / p' ; q is deviatoric stress.

2.2 Error Analysis of the Proposed Anisotropic Yield Surface for Sands

To verify the applicability of the proposed anisotropic yield surface for sands, the experimental yield data of anisotropically consolidated Aio sand reported by Yasufuku et al. (1991) were selected. In their study, a series of triaxial tests were conducted under different initial anisotropies and stress levels to investigate the yielding characteristics of sand. Four groups of specimens were tested in total: two groups of specimens with an initial stress ratio

of $\eta = 0.8$ under low and high stress levels, respectively, and two additional groups of specimens with stress ratios of $\eta = 0$ and $\eta = -0.8$ under low stress levels. The yield points obtained from these four groups of specimens provide a comprehensive basis for evaluating the yielding behavior of sand under different consolidation states and loading directions, offering reliable experimental data for the error analysis of the proposed model.

Four yield surface formulations, namely Eqs. (4), (5), (7) and (8), were employed to simulate the experimental yield loci. For each experimental yield point, a radial line was drawn through the quasi-center point (located at $\text{demi-}p_{c0}$ on the α_0 -line) and the experimental point, and its intersection with the theoretical yield surface was determined. The relative error was defined as the ratio of the distance Δ_i between the intersection and the experimental point to the radius R_i from the quasi-center point to the intersection. The standard error (SE) was calculated as $SE = \sqrt{\sum_N (\Delta_i / R_i)^2 / N}$ with N the total number of experimental yield points. Table 1 shows the parameters corresponding to the four yield surface formulations used for fitting the experimental data. The comparisons between the experimental data and the theoretical yield surfaces obtained from the four new formulations are illustrated in Fig. 3, where the results corresponding to Eqs. (4), (5), (7) and (8) are shown sequentially. The associated standard errors for different yield surfaces are summarized in Fig. 4. The results show that the proposed anisotropic yield surface can reasonably reproduce the experimental yield curves under different loading conditions, with overall good agreement. Among the four formulations, those defined by Eqs. (4) and (7) provide higher fitting accuracy, indicating that the inclusion of both the shape parameters n and χ effectively enhances the model's

ability to describe the anisotropic yielding behavior of sands under complex stress paths. For clarity and simplicity, the subsequent model development and validation are based solely on Eq. (4), although Eq. (4) may be replaced by alternative formulations if required.

Table 1 Parameters and initial state variables for four yield surface formulations used for fitting

Parameters	M_c / M_e	n	χ	α_0
Eq. (4)			0.26	
Eq. (5)	1.30 / 0.90	1.2	0.20	0.5, 0.5, 0 and -0.3
Eq. (7)			0.29	for Test 1-4
Eq. (8)			0.20	

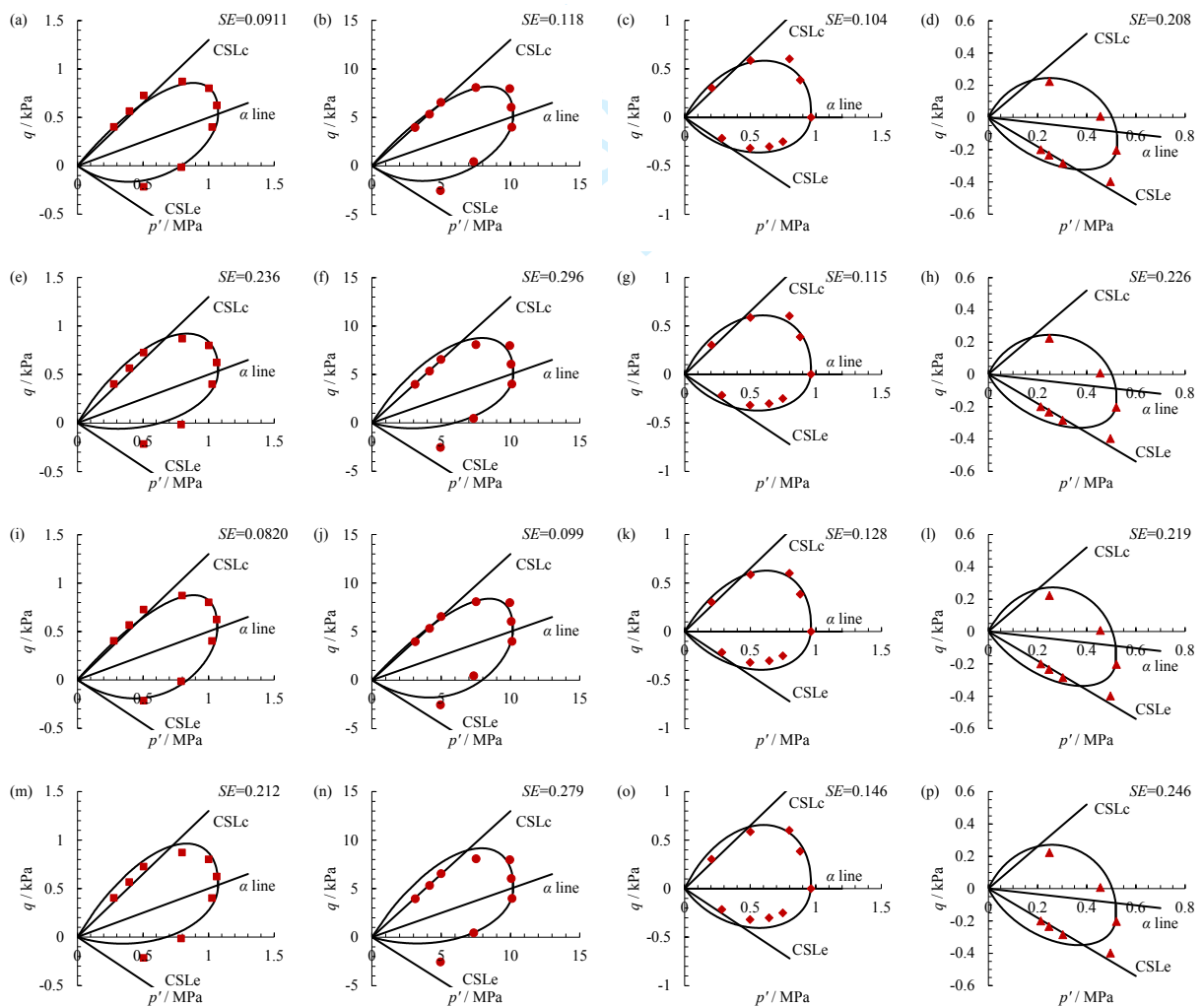


Fig. 3 Comparison between experimental data and theoretical curves by the four new formulation for sand

by (a-d) Eq. (4), (e-h) Eq. (5), (i-l) Eq. (7) and (m-p) Eq. (8)

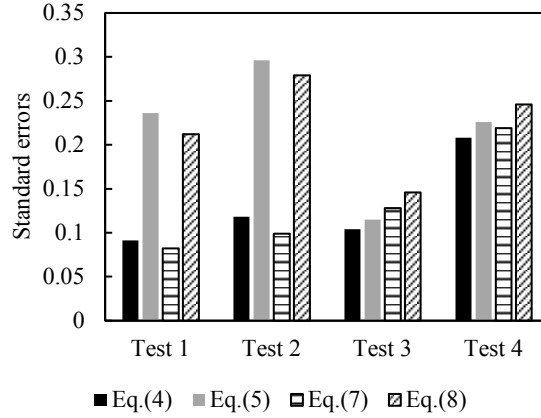


Fig. 4 Comparisons of standard errors by different surfaces for sand

3. Elasto-Plastic Model of Sands

According to elasto-plasticity theory, the total strain increment tensor is additively decomposed into elastic and plastic components:

$$d\boldsymbol{\varepsilon} = d\boldsymbol{\varepsilon}^e + d\boldsymbol{\varepsilon}^p \quad (11)$$

where $d\boldsymbol{\varepsilon}$ is the total strain increment tensor, and superscripts e and p denote the elastic and plastic parts, respectively.

3.1 Elastic Law

The elastic behavior of sand is assumed to be isotropic:

$$d\boldsymbol{\varepsilon}^e = \frac{1+\nu}{E} d\boldsymbol{\sigma}' - \frac{3\nu}{E} dp' \boldsymbol{\delta} \quad (12)$$

where $\boldsymbol{\sigma}'$ is the effective stress tensor; p' is the mean effective stress; ν is Poisson's ratio; E is Young's modulus. The modulus E may be replaced by the elastic bulk modulus K using the relation $E = 3K(1-2\nu)$. The swelling line for sand is typically considered to be linear in either the $\log e - \log p'$ plane or the $e - \log p'$ plane. The elastic

bulk modulus K is defined as $K = p'(1+e_0)/(\kappa'e) = p'(1+e_0)/\kappa e$, where κ' and κ are the slopes of the swelling line in the $\log e - \log p'$ plane and the $e - \log p'$ plane, respectively, and e is the void ratio. The relationship between κ' and κ is given by $\kappa' = \kappa/e$. In the following, the parameter κ' is used to calculate the elastic stress-strain relationship. Depending on the specific case, κ' can either be determined from the slope of the swelling line in the $\log e - \log p'$ plane or calculated from the known value of κ .

3.2 Non-Associative Flow Rule

The plastic potential function g is taken as a simplified version of the yield surface with fixed parameters $n = 1$ and $\chi = 0$, resulting in a non-associative flow rule:

$$g = \frac{M - \alpha \frac{3}{2}(\mathbf{r} - \boldsymbol{\alpha}_d) : (\mathbf{r} - \boldsymbol{\alpha}_d)}{M + \alpha (M - \alpha)^2} p' + p' - p_c \quad (13)$$

3.3 Anisotropic Bounding Surface Model

The model is established within the unified hardening (UH) framework based on the bounding surface concept (Dafalias and Herrmann 1982), as formulated by Yao et al. (2009). When the isotropic consolidation line (ICL) for sand is considered to be linear in the $\log e - \log p'$ plane, the hardening rule can be replaced by:

$$dp_c = p_c \frac{1+e}{(\lambda' - \kappa')e} dH_v \quad \text{with} \quad dH_v = \frac{1}{\Omega} d\varepsilon_v^p \quad (14)$$

where the parameter λ' controls the slope of the compression line at high stress levels in the double logarithmic $\log e - \log p'$ plane. When the slope λ of the isotropic consolidation line in the $e - \log p'$ plane is known, λ' can be determined using the relation $\lambda' = \lambda/e$. Ω considering small strain stiffness is defined as follows according to Yao et al. (2016):

$$\Omega = R^{k(M_f - \eta)} \frac{M^8 - \eta^8}{M_f^8 - \eta^8} \quad (15)$$

$$M_f = 6 \left[\sqrt{\frac{k}{R} \left(1 + \frac{k}{R} \right)} - \frac{k}{R} \right] \quad (16)$$

$$k = \frac{M^2}{12(3 - M)} \quad (17)$$

$$\left\{ \begin{array}{l} R = \left\{ \frac{M - \alpha}{nM + \alpha} \left[\frac{(1 + \chi)^{\frac{3}{2}} (\mathbf{r} - \boldsymbol{\alpha}_d) : (\mathbf{r} - \boldsymbol{\alpha}_d)}{(M - \alpha)^2 - \chi \left(\frac{3}{2} \mathbf{r} : \mathbf{r} - \frac{3}{2} \boldsymbol{\alpha}_d : \boldsymbol{\alpha}_d \right)} \right]^{\frac{n+1}{2}} + 1 \right\} \frac{p'}{\bar{p}_c} \text{ for Eq. (4)} \\ R = \left\{ \frac{M - \alpha}{nM + \alpha} \left[\frac{(1 + \chi)^{\frac{3}{2}} (\mathbf{r} - \boldsymbol{\alpha}_d) : (\mathbf{r} - \boldsymbol{\alpha}_d)}{(M - \alpha)^2 - \chi \frac{3}{2} (\mathbf{r} - \boldsymbol{\alpha}_d) : (\mathbf{r} - \boldsymbol{\alpha}_d)} \right]^{\frac{n+1}{2}} + 1 \right\} \frac{p'}{\bar{p}_c} \text{ for Eq. (5)} \end{array} \right. \quad (18)$$

$$d\bar{p}_c = \bar{p}_c \frac{1 + e}{(\lambda' - \kappa')e} d\varepsilon_v^p \quad (19)$$

where parameter k controls the effect of over-consolidation ratio to small strain stiffness.

For modeling induced anisotropy, various rotational hardening laws have been proposed in the literature (e.g., Ling et al. 2002; Wheeler et al. 2003; Dafalias and Taiebat 2013). The rotational hardening law proposed by Wheeler et al. (2003) was simply adopted, i.e.,

$$d\boldsymbol{\alpha}_d = \omega \left[\left(a \frac{\boldsymbol{\sigma}_d}{p'} - \boldsymbol{\alpha}_d \right) \langle d\varepsilon_v^p \rangle + \omega_d \left(b \frac{\boldsymbol{\sigma}_d}{p'} - \boldsymbol{\alpha}_d \right) d\varepsilon_d^p \right] \quad (20)$$

where ω controls the rate at which the inclination evolves with plastic strain, ω_d governs the contribution of plastic deviatoric strain to the inclination evolution, and the parameters a and b define the target values of $\boldsymbol{\alpha}_d$ at large plastic volumetric and deviatoric strains, respectively. The MacCauley function $\langle d\varepsilon_v^p \rangle = (d\varepsilon_v^p + |d\varepsilon_v^p|)/2$ is used to ensure one-sided evolution. For simplicity, the subsequent validation assumes $\omega_d = 1$ and $a = b = 0$.

The plastic strain increment on the current surface for each incremental step can be expressed as

$$d\boldsymbol{\varepsilon}^p = \Lambda \frac{\partial \mathbf{g}}{\partial \boldsymbol{\sigma}} \quad (21)$$

where the plastic multiplier Λ can be derived from the consistency condition of the current surface in this incremental step

$$\Lambda = \frac{-\frac{\partial f}{\partial p'} dp' - \frac{\partial f}{\partial \boldsymbol{\sigma}_d} : d\boldsymbol{\sigma}_d}{\frac{1}{\Omega} \frac{\partial f}{\partial p_c} \frac{\partial p_c}{\partial \varepsilon_v^p} \frac{\partial g}{\partial p'} + \frac{\partial f}{\partial \boldsymbol{\alpha}_d} : \frac{\partial \boldsymbol{\alpha}_d}{\partial \varepsilon_d^p} \left| \frac{\partial g}{\partial q} \right|} \quad (22)$$

With this, the stress–strain relationship can be fully determined.

3.4 Summary of Model Parameters

The model parameters and initial state variables are categorized into three groups:

- (1) Cam-Clay parameters and state variables: ν , κ' , λ' , M and p_{c0} .
- (2) Yield surface shape parameters: n and χ , determined from anisotropic consolidation or undrained triaxial tests.
- (3) Initial and induced anisotropy parameters: α_0 and ω , calibrated using the $\varepsilon_a - q$ curve.

4. Test Simulations

To evaluate the effectiveness of the proposed yield surfaces, a series of validation studies is conducted. First, using one selected yield function, a systematic analysis is carried out to investigate how the degradation of the shape parameters n and χ and the anisotropic state variable α affects the model response. Second, sensitivity analysis is performed to quantify the impact of key model parameters on the overall response.

4.1 Comparative Analysis of Degraded Yield Surfaces

The undrained shear behavior of very loose Hostun sand under K_0 -consolidated

To comprehensively evaluate the performance of the proposed yield surface defined by Eq. (4), predictions from constitutive models incorporating four different yield surface formulations are compared. These four configurations are defined as follows: 1) a baseline model without the shape parameter n and χ or the anisotropic state variable α ; 2) a model including only the shape parameter n and χ ; 3) a model including only the anisotropic state variable α ; and 4) a model incorporating both n , χ and α .

The model parameters and initial state variables used for predicting the triaxial shear behavior of Hostun sand are summarized in Table 2. Parameters associated with the Cam-Clay model are adopted from the values reported by Dubujet and Doanh (1997) and Yin et al. (2009). The initial values of the anisotropy state variable were assigned as $\alpha_0 = 0, 0.33,$ and 0.56 for specimens consolidated at $K_0 = 1.0, 0.66,$ and $0.5,$ respectively. These values were estimated following Wheeler's rotational hardening framework, in which volumetric viscoplastic strains drive the anisotropy toward approximately $3/4\eta$. Accordingly, the initial anisotropy was approximated as $\alpha_0 \approx 0.75\eta_c$, where $\eta_c = q/p'$ is the constant stress ratio applied during anisotropic consolidation. The parameters n, χ and ω are calibrated using the optimization method proposed by Jin et al. (2016, 2017). Calibration is based on six undrained triaxial tests conducted under the following conditions: ($K_0 = 1.0, p'_0 = 400$ kPa), ($K_0 = 0.66, p'_0 = 400$ kPa), and ($K_0 = 0.5, p'_0 = 300$ kPa), covering both compression and extension modes.

Table 2 Parameters and initial state variables for elasto-plastic models with degraded yield surfaces

Parameters	ν	κ	λ	M_c	n	χ	ω
Type 1					1	0	--
Type 2	0.2	0.01	0.07	1.33	1.1	0.85	--
Type 3					1	0	100
Type 4					1.1	0.85	100

Note: Type 1–4 correspond to different yield surface formulations as defined above.

Fig. 6 - Fig. 8 present comparisons between experimental data and model predictions for undrained triaxial compression and extension tests on loose sand specimens subjected to both isotropic and anisotropic consolidation. In this study, the deviatoric stress is defined as $q = \sigma_a - \sigma_r$. Under triaxial extension conditions, this definition may lead to negative values of q when the axial stress becomes smaller than the radial stress. The following section first examines the complex shear behavior of loose sand under different consolidation and shear conditions. As shown in Fig. 6(a), the stress–strain response of isotropically consolidated very loose sand exhibits a pronounced drop in deviatoric stress immediately after reaching the peak. Maximum compression and minimum extension typically occur at the onset of the undrained loading stage, with peak axial strain values around $\pm 0.5\%$. This initial softening is followed by a relatively stable phase in which the residual strength remains nearly constant across a wide range of axial strains. In some cases, the deviatoric stress may exhibit a slight post-peak increase, occurring beyond $+8\%$ axial strain in compression or -6% in extension, which may be attributed to an underestimation of surface effects in the absence of an anti-friction system. Moreover, the peak deviatoric stress and the corresponding axial strain

are both influenced by the initial isotropic confining pressure. Specifically, higher confining pressures lead to greater peak strength and correspondingly larger axial strains at the peak.

Fig. 6(b) illustrates the effective stress paths in the $p'-q$ plane. Initiating from isotropic stress conditions, both the compression and extension paths form a closed trajectory directed toward the origin, with slight asymmetry about the hydrostatic axis. The stress paths under varying confining pressures intersect the isotropic consolidation axis nearly perpendicularly, indicating minimal changes in p' and suggesting predominantly elastic behavior during the early stages of shearing.

In compression tests on anisotropically consolidated samples, Fig. 6(c) and Fig. 6(e) show a more pronounced drop in deviatoric stress immediately following a relatively minor peak, indicating a greater post-peak strength reduction compared to isotropic cases. The difference between the peak deviatoric stress and the residual stress at the end of the test increases with higher consolidation pressure at a given stress ratio K_0 , and decreases as K_0 is reduced under the same consolidation pressure. The axial strain corresponding to the peak stress is significantly smaller than that observed in isotropic samples—ranging from 0.1% to 0.2% for $K_0 = 0.66$, and from 0.02% to 0.04% for $K_0 = 0.5$. Moreover, in extension tests, the deviatoric stress also exhibits a local minimum, followed by a slight increase toward a negative residual strength. The axial strain at peak deviatoric stress in extension is larger than in compression, typically ranging from -0.4% to -1.5% , and increases with the level of final consolidation pressure.

As shown in Fig. 6(d) and Fig. 6(f), the effective stress paths of anisotropically consolidated specimens exhibit geometric similarity. Under low consolidation pressures, the compression stress paths remain approximately perpendicular to the hydrostatic axis. However, all stress paths show pronounced asymmetry with respect to the consolidation axis. Above the constant consolidation line, the paths become more elongated and deviate from perpendicularity. Below the line, this deviation increases further and the protuberance is shifted away from the origin of the axes. Notably, the transition from compression to extension, originating from the anisotropic consolidated state, progresses in a smooth and continuous manner.

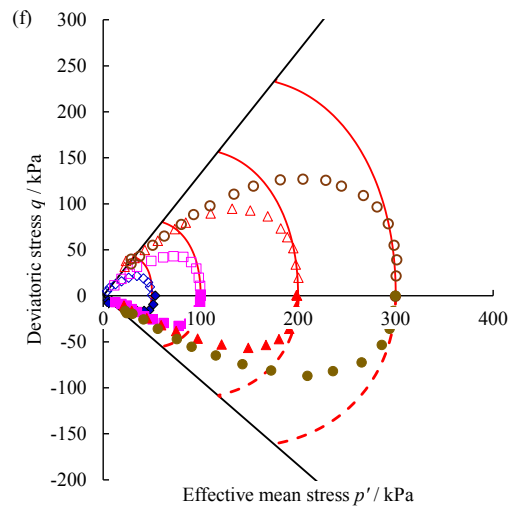
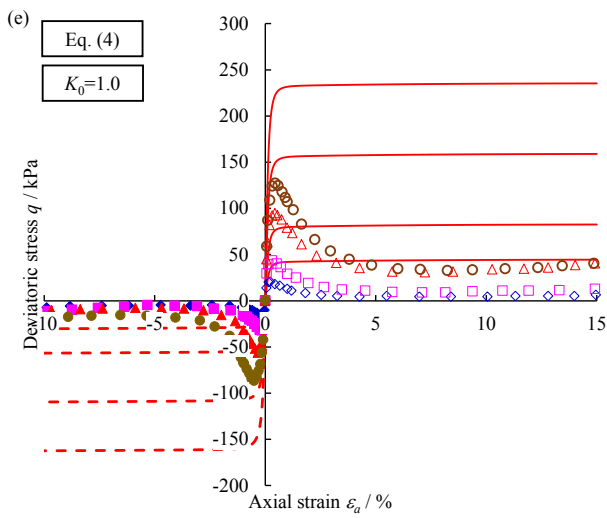
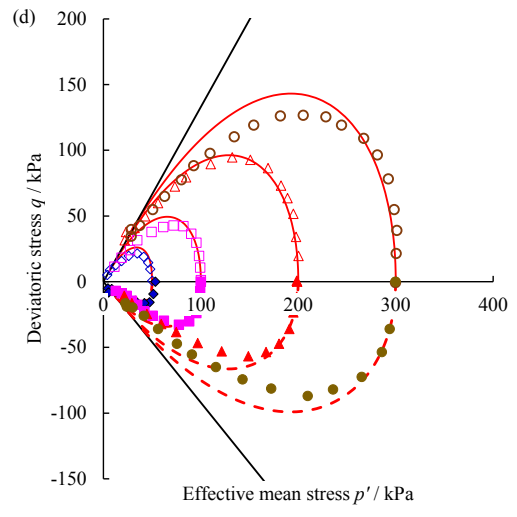
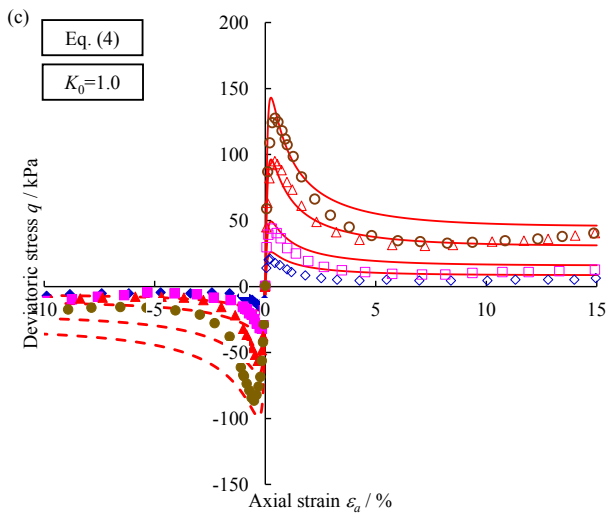
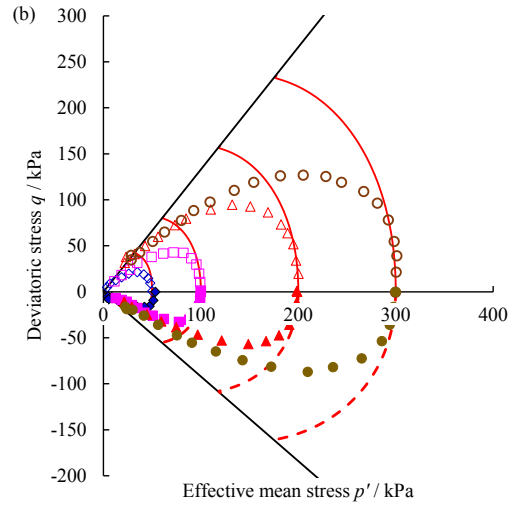
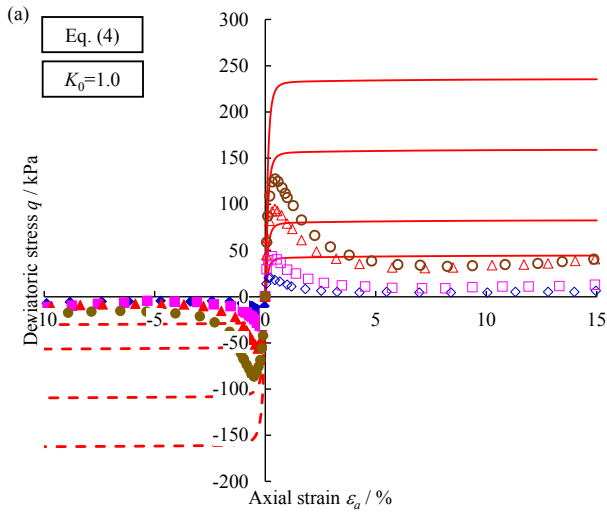
As noted earlier, the shear behavior of loose sand in undrained triaxial tests is highly complex, underscoring the difficulty of accurately reproducing its response under various consolidation and shearing conditions. This section therefore evaluates and compares the predictive performance of the proposed models using the proposed yield surface formulation and its degenerated forms. For isotropically consolidated specimens, the two models that exclude the shape parameters n and χ fail to capture the post-peak softening observed in both triaxial compression and extension tests, as illustrated in Fig. 6(a), (b), (e), and (f). In contrast, incorporating n and χ yields consistently satisfactory predictions of undrained compression and extension behavior, as shown in Fig. 6(c), (d), (g), and (h).

A similar trend is observed for anisotropically consolidated specimens with $K_0 = 0.66$ and 0.5. As shown in Fig. 7(a), (b) and Fig. 8(a), (b), the model without the shape parameters n , χ , and the anisotropic variable α remains unable to reproduce the softening response in

compression and extension. When only the shape parameters (n, χ) are included (Fig. 7(c), (d); Fig. 8(c), (d)), the model is able to reproduce the softening behavior; however, the predicted effective stress paths in triaxial extension start nearly vertical and exhibit a very rapid change in the deviatoric stress q , changing from positive values to zero and then further into the negative range, which is inconsistent with the experimental observations.

Including only the anisotropic variable α improves the initial portion of the effective stress path under extension loading (Fig. 7(e), (f); Fig. 8(e), (f)), but the predicted softening behavior in both compression and extension remains inadequate. By contrast, when n, χ , and α are introduced simultaneously, the model achieves robust and accurate predictions for both loading modes, as demonstrated in Fig. 7(g), (h) and Fig. 8(g), (h).

Overall, these comparisons show that for $K_0=1$, using only the shape parameters n and χ yields reasonable predictions, whereas for lower K_0 values, models relying solely on n and χ or solely on the anisotropic state variable α cannot fully reproduce the complex stress–strain responses in compression and extension. Incorporating n, χ , and α together substantially improves model performance, indicating that these parameters are essential for describing the yield-surface geometry and the mechanical behavior of K_0 -consolidated sands. While the overall predictive capacity is satisfactory, some discrepancies remain, partly because the present formulation employs a simplified plastic potential function and a simplified anisotropic hardening law. Continued refinement of these components, such as adopting a more realistic flow rule and a more comprehensive anisotropic hardening scheme, may further enhance predictive accuracy.



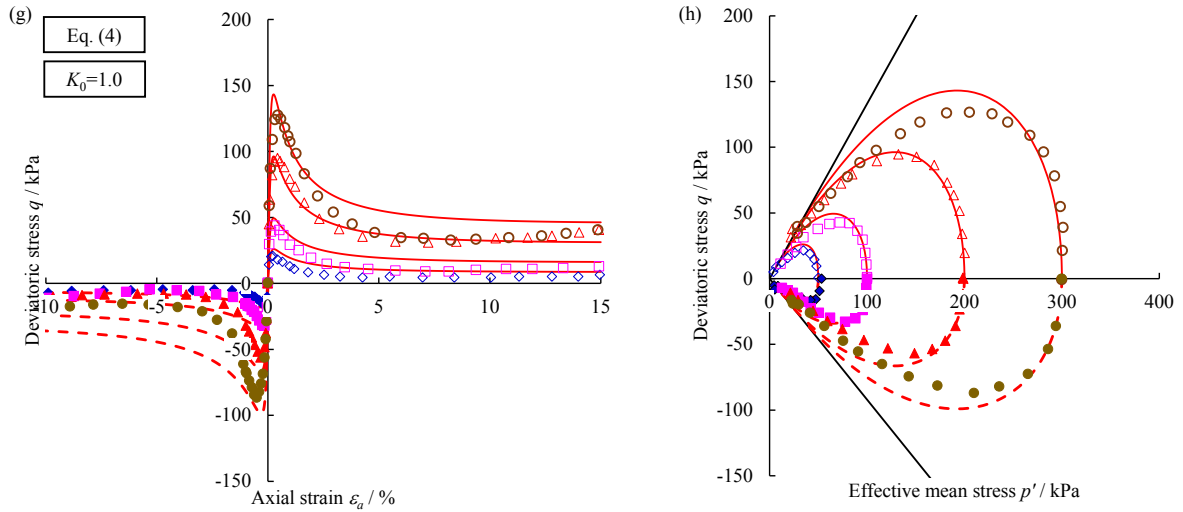
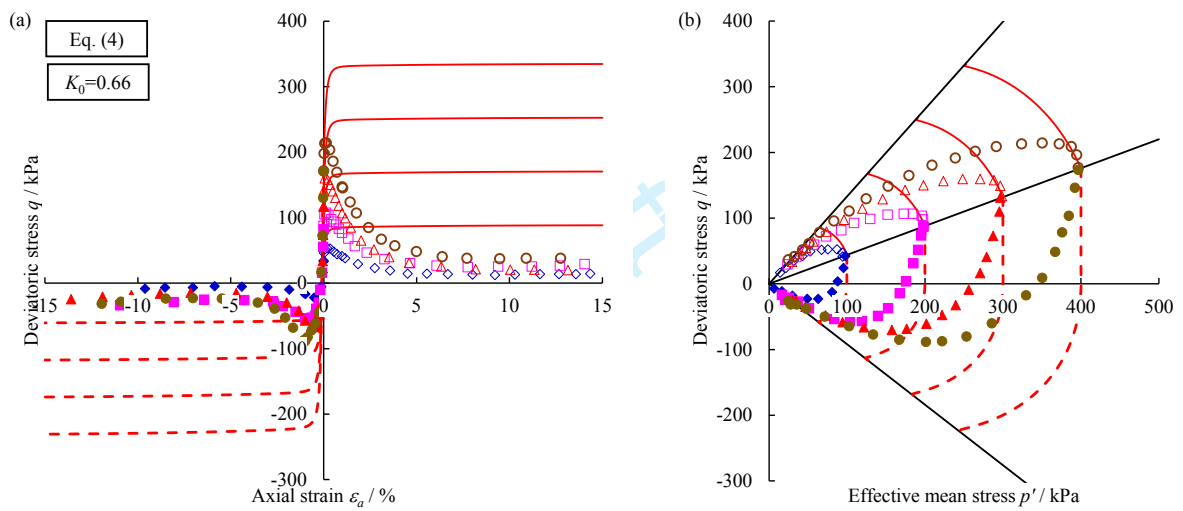


Fig. 6 Influence of yield surface shape and anisotropy on predicted results of undrained triaxial shear tests for anisotropic consolidated Houtun sand with $K_0 = 1$ in the ϵ_a - q and p' - q planes: (a) and (b) without n , χ and α ; (c) and (d) with n and χ ; (e) and (f) with α ; (g) and (h) with n , χ and α



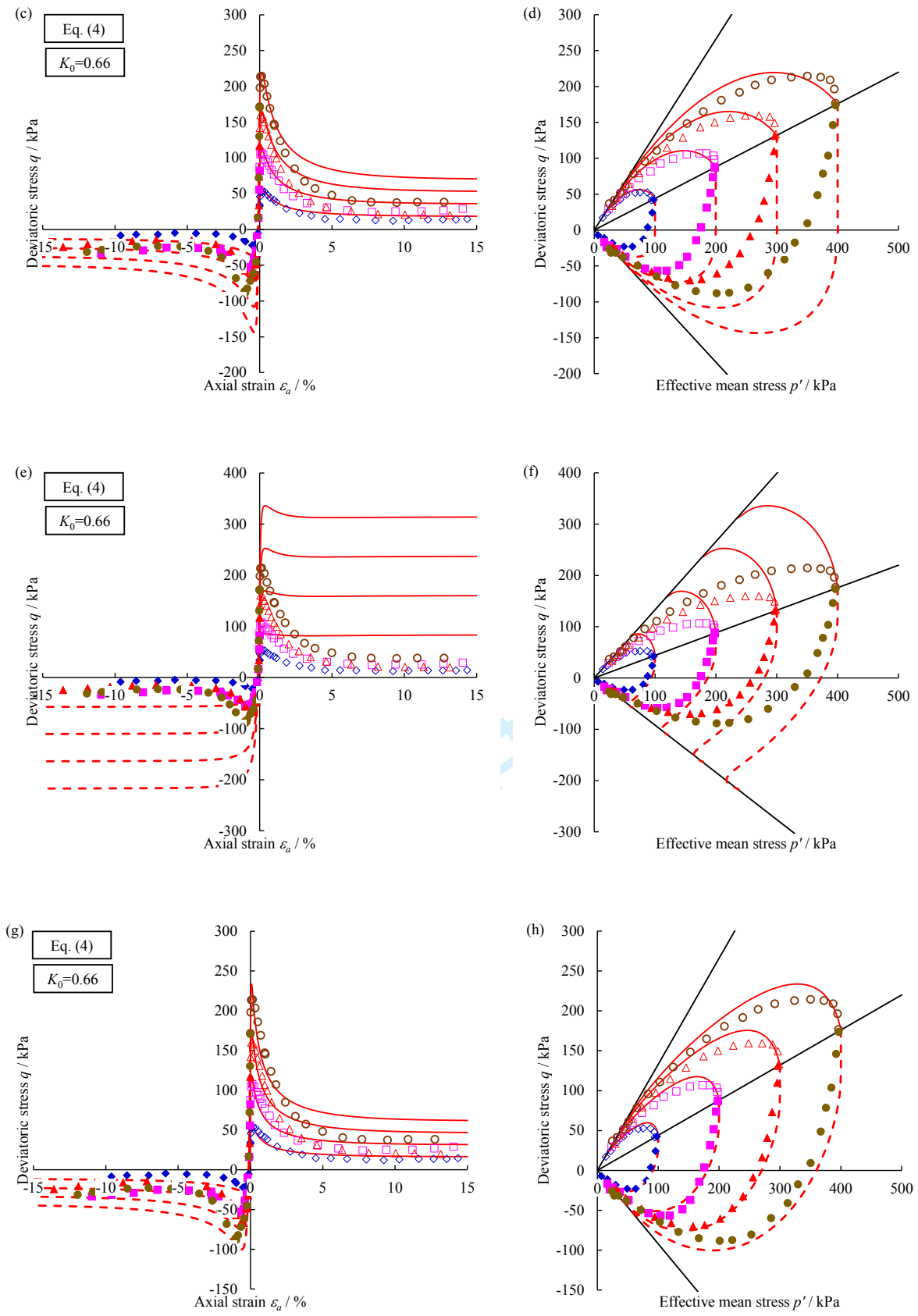
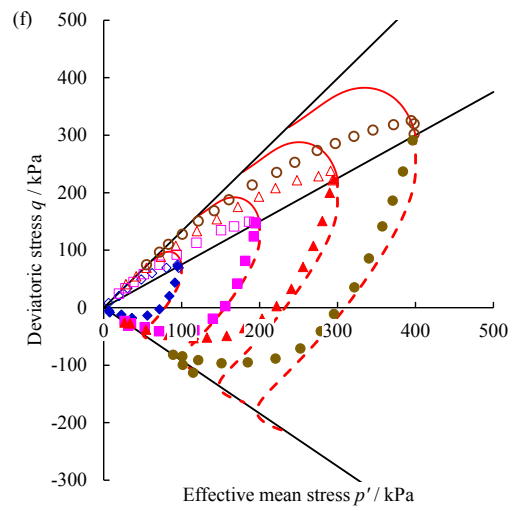
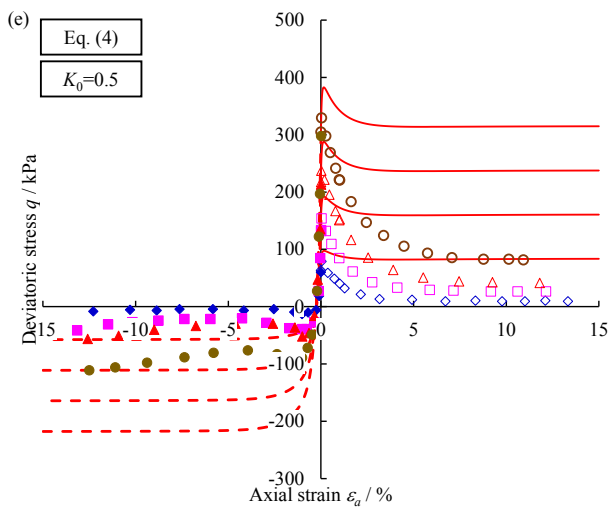
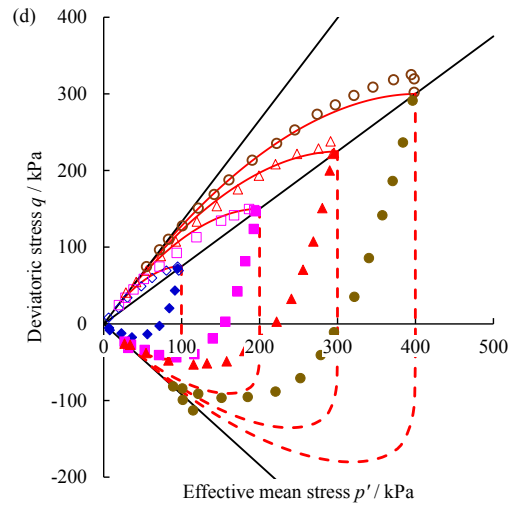
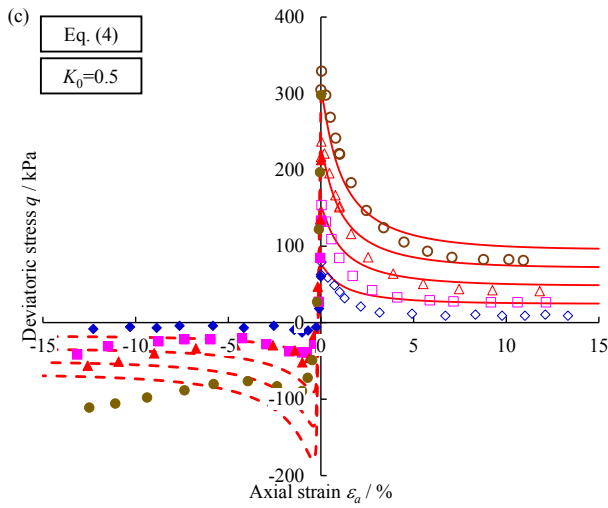
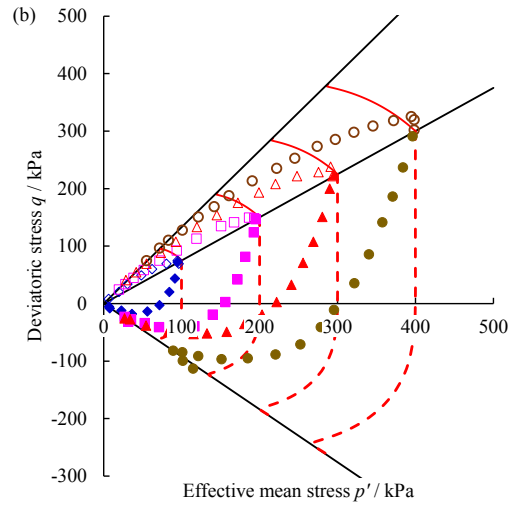
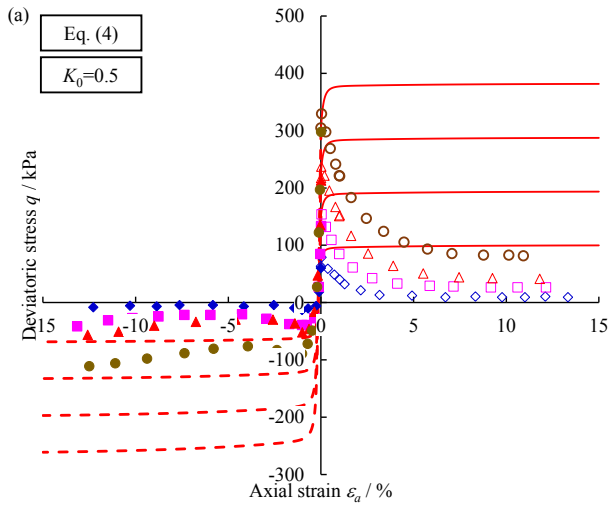


Fig. 7 Influence of yield surface shape and anisotropy on predicted results of undrained triaxial shear tests for anisotropic consolidated Houtun sand with $K_0 = 0.66$ in the ϵ_a - q and p' - q planes: (a) and (b) without n ,

χ and α ; (c) and (d) with n and χ ; (e) and (f) with α ; (g) and (h) with n , χ and α



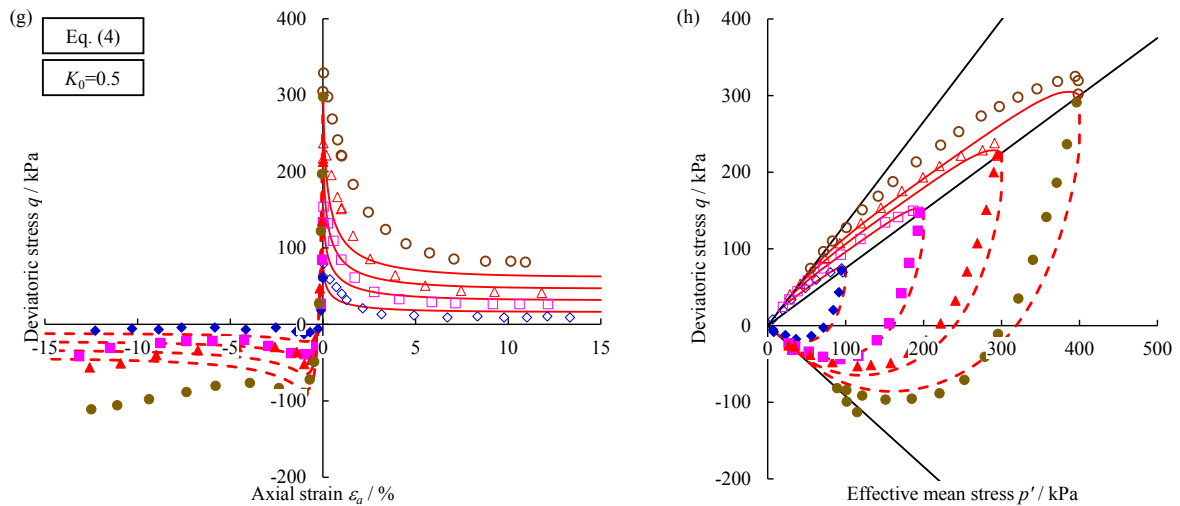


Fig. 8 Influence of yield surface shape and anisotropy on predicted results of undrained triaxial shear tests for anisotropic consolidated Houtun sand with $K_0 = 0.5$ in the ϵ_a - q and p' - q planes: (a) and (b) without n , χ and α ; (c) and (d) with n and χ ; (e) and (f) with α ; (g) and (h) with n , χ and α

4.2 Comparative Analysis of Parameter Sensitivity

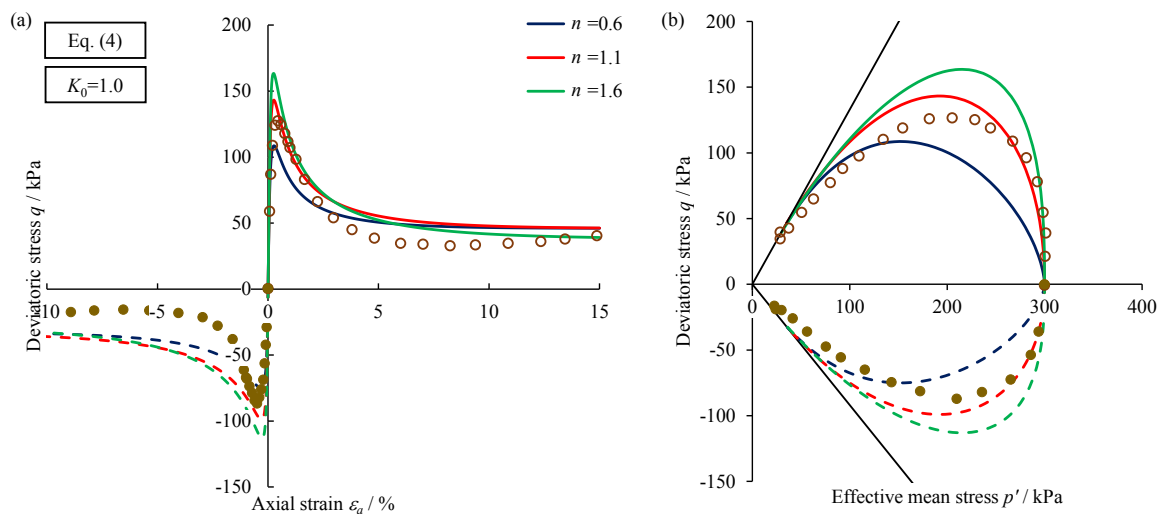
The influences of three model parameters— n , χ and ω —on the predicted undrained triaxial behavior were investigated. Simulations were conducted for isotropically and anisotropically consolidated specimens with stress ratios of $K_0 = 1, 0.66$ and a consolidation pressure of $p'_0 = 400$ kPa. The predicted stress–strain responses and effective stress paths for different parameter values are shown in Fig. 9-Fig. 11.

Fig. 9 shows the predicted results for varying values of the shape parameter $n = 0.6, 1.1, 1.6$, while keeping $\chi = 0.85$ and $\omega = 100$ constant. As illustrated in Fig. 1(a), increasing the value of n causes the right half of the yield surface to expand and the left half to contract. Consequently, the intersection of the upper half of the yield surface with the critical state line in compression (CSLc) shifts upward and rightward, while the intersection with the critical

state line in extension (CSLe) remains largely unchanged. As a result, higher values of n lead to increased predicted peak deviatoric stress in both triaxial compression and extension tests.

Fig. 10 presents the predicted responses for varying values of the shape parameter $\chi = 0.7, 0.85, 1.0$, with $n = 1.1$ and $\omega = 100$ held constant. As shown in Fig. 1(b), increasing χ causes the yield surface to gradually flatten into a droplet shape. The intersection point between the yield surface and the critical state line shifts toward the origin, eventually coinciding with it. Accordingly, as χ increases, both the predicted peak and residual deviatoric stresses decrease in both triaxial compression and extension tests.

Fig. 11 display the predicted responses for varying values of the parameter $\omega = 50, 100, 200$, with $n = 1.1$ and $\chi = 0.85$ held constant. As described in Eq. (20), the parameter ω controls the rate at which anisotropy evolves during the shearing process. As ω increases, the evolution of anisotropy accelerates. As a result, the predicted peak compressive strength decreases, while the peak extensive strength slightly increases. The residual strength, however, remains virtually unaffected by changes in ω .



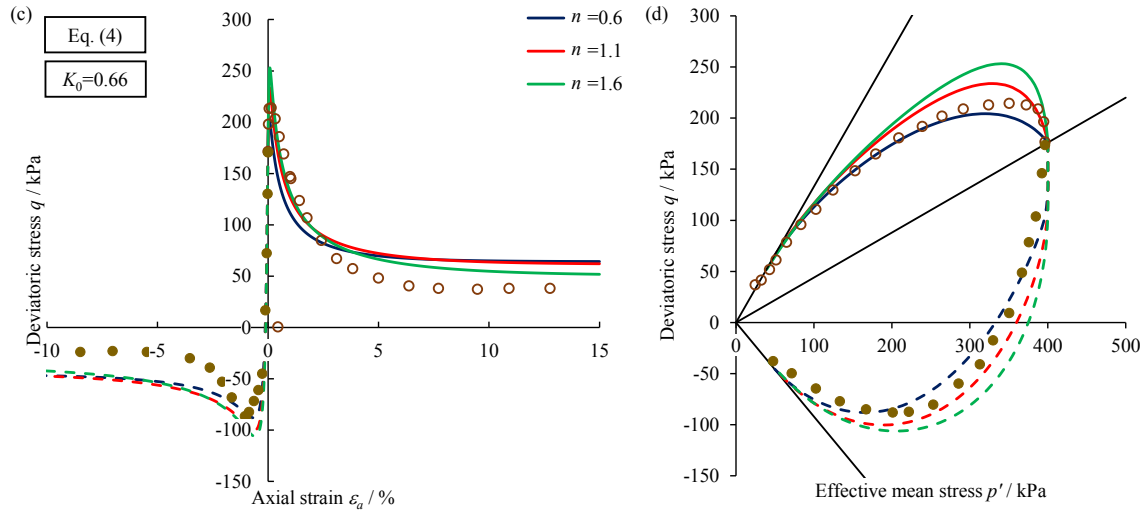


Fig. 9 Influence of model parameter n on predicted results of undrained triaxial shear tests for (a), (b) isotropically and (c), (d) anisotropically consolidated Hostun sand with $K_0 = 1, 0.66$ and $p'_0 = 400$ kPa in the $\epsilon_a - q$ and $p' - q$ planes

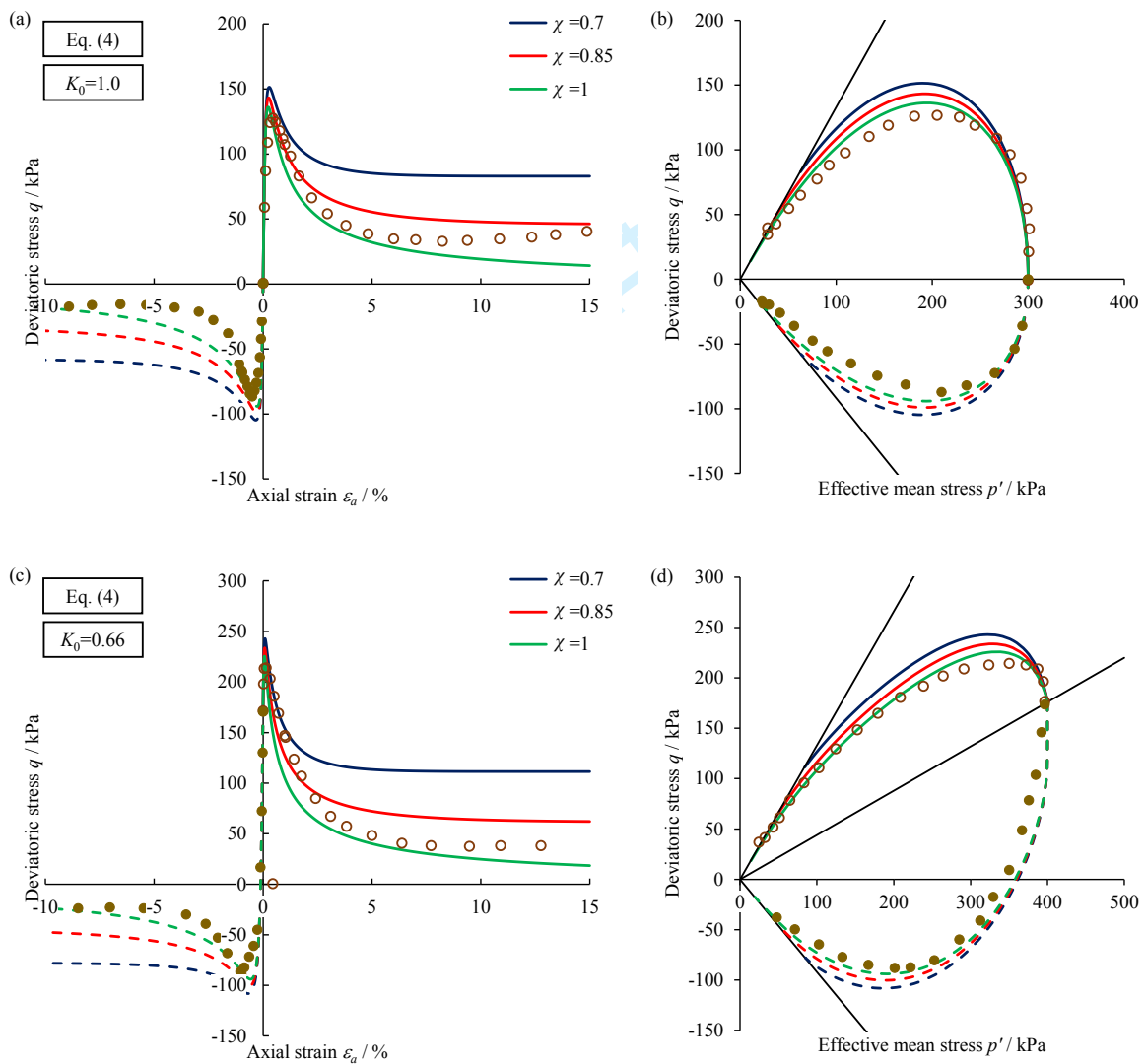


Fig. 10 Influence of model parameter χ on predicted results of undrained triaxial shear tests for (a), (b) isotropically and (c), (d) anisotropically consolidated Hostun sand with $K_0 = 1, 0.66$ and $p'_0 = 400$ kPa in the $\varepsilon_a - q$ and $p' - q$ planes

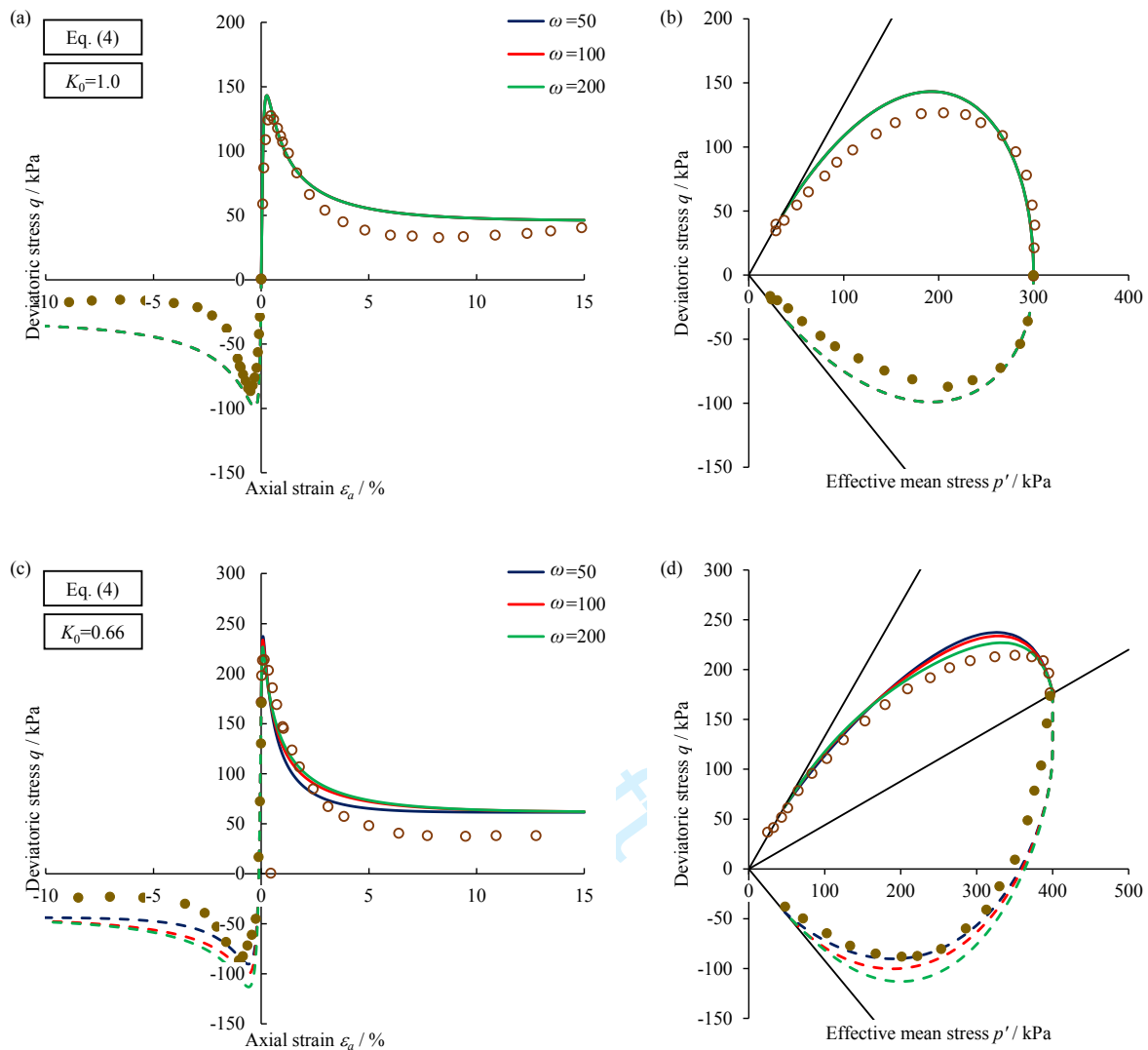


Fig. 11 Influence of model parameter ω on predicted results of undrained triaxial shear tests for (a), (b) isotropically and (c), (d) anisotropically consolidated Hostun sand with $K_0 = 1, 0.66$ and $p'_0 = 400$ kPa in the $\varepsilon_a - q$ and $p' - q$ planes

5. Conclusion

In this study, some anisotropic yield surface were proposed to model the shear behavior of K_0 -consolidated sands, extending the flexible anisotropic yield function developed by Yin and Li (2025) for K_0 -consolidated clays. The proposed yield surfaces incorporate two key shape parameters n and χ and one anisotropic state variable α , offering flexibility in

controlling the shape of the yield surface. These parameters improve the model's ability to capture the shear response under both compression and extension conditions. As n increases, the yield surface expands asymmetrically, with the right half enlarging and the left half contracting. Meanwhile, χ primarily influences the flattening of the yield surface into a droplet shape. These geometric changes affect the stress–strain response across different loading paths.

The effectiveness of the proposed yield surfaces was assessed through three complementary studies within a bounding surface plasticity framework, validated against undrained triaxial compression and extension tests on very loose Hostun sand as reported by Doanh et al. (1997). First, a systematic analysis of the degraded yield surfaces was conducted using four model configurations: (1) without parameters n , χ and α ; (2) including only n and χ ; (3) including only α ; and (4) including both n , χ and α . Overall, these comparisons indicate that when $K_0 = 1$, incorporating only the shape parameters n and χ already yields reasonable predictions, whereas for lower K_0 values, models using only n and χ or only the anisotropic variable α fail to capture the complex stress–strain responses. In contrast, the combined inclusion of n , χ , and α markedly improves prediction accuracy, confirming that these three parameters are essential for defining the yield-surface geometry and for reproducing the mechanical behavior of K_0 -consolidated sands.

Second, a parameter sensitivity analysis was conducted to examine how the key model parameters influence predictive performance. The results show that the shape parameters n and χ primarily determine the geometry of the yield surface, which in turn governs both peak

and residual strengths. Increasing n enhances the predicted peak strengths, whereas increasing χ reduces them by flattening the surface. The parameter ω mainly controls the rate of anisotropy development during shearing, and larger values of ω lower the peak compressive strength and slightly increase the peak extensive strength, while leaving the residual strength nearly unchanged. These findings confirm that the shape parameters n and χ , along with the anisotropic state variable α , play a critical role in defining the yield surface geometry and enhancing the model's capability to simulate the complex behavior of K_0 -consolidated sands.

Competing Interests Statement

The authors declared that they have no conflicts of interest to this work. We declare that we do not have any commercial or associative interest that represents a conflict of interest in connection with the work submitted.

Data Availability Statement

All data, models, and code generated or used during the study appear in the submitted article.

Acknowledgments

The financial supports provided by the National Natural Science Foundation of China (Grant No. 52278324), the Fundamental Research Funds for the Central Universities (Grant No. 2023JBMC048) and the Research Grants Council (RGC) of Hong Kong Special Administrative Region Government (HKSARG) of China (Grant No. 15232224, 15227923, 15220221) are gratefully acknowledged.

Reference

- Asaoka, A., Noda, T., Yamada, E., Kaneda, K. and Nakano, M. 2002. An elasto-plastic description of two distinct volume change mechanisms of soils. *Soils and Foundations*. **42**(5): 47-57. doi:10.3208/sandf.42.5_47.
- Dafalias, Y.F., and Herrmann, L.R. 1982. Bounding surface formulation of soil plasticity. In *Soil mechanics: Transient and cyclic loads*. Edited by G.N. Pande and O.C. Zienkiewicz. John Wiley & Sons, Chichester. pp. 253-282.
- Dafalias, Y.F., and Taiebat, M. 2013. Anatomy of rotational hardening in clay plasticity. *Géotechnique*. **63**(16): 1406-1418. doi:10.1680/geot.12.P.197.
- Doanh, T., Ibraim, E., and Matiotti, R. 1997. Undrained instability of very loose Hostun sand in triaxial compression and extension. Part 1: experimental observations. *Mechanics of Cohesive-Frictional Materials*, **2**: 47-70.
doi:10.1002/(SICI)1099-1484(199701)2:1<47::AID-CFM26>3.0.CO;2-9.
- Dubujet, Ph., and Doanh, T. 1997. Undrained instability of very loose Hostun sand in triaxial compression and extension. Part 2: theoretical analysis using an elastoplasticity model. *Mechanics of Cohesive-Frictional Materials*, **2**: 71-92.
doi:10.1002/(SICI)1099-1484(199701)2:1<71::AID-CFM25>3.0.CO;2-9.
- Jin, Y.-F., Yin, Z.-Y., Shen, S.-L., and Hicher, P.-Y. 2016. Selection of sand models and identification of parameters using an enhanced genetic algorithm. *International Journal for Numerical and Analytical Methods in Geomechanics*, **40**(8): 1219-1240.
doi:10.1002/nag.2487.
- Jin, Y.-F., Yin, Z.-Y., Riou, Y., and Hicher, P.-Y. 2017. Identifying creep and destructuration related soil parameters by optimization methods. *KSCE Journal of Civil Engineering*, **21**(4): 1123-1134. doi:10.1007/s12205-016-0378-8.
- Landivar Macias, A., and Rotta Loria, A. F. 2023. SANISAND-C*: Simple ANIsotropic

- constitutive model for SAND with Cementation. *International Journal for Numerical and Analytical Methods in Geomechanics*. **47**: 2815-2847. doi:10.1002/nag.3602.
- Li, X. S., and Dafalias, Y. F. 2000. Dilatancy for cohesionless soils. *Géotechnique*. **50**(4): 449-460. doi:10.1680/geot.2000.50.4.449.
- Liang, R.-Y., and Shaw H.-L. 1991. Anisotropic hardening plasticity model for sands. *Journal of Geotechnical Engineering (ASCE)*. **117**(6): 913-931. doi:10.1061/(ASCE)0733-9410(1991)117:6(913).
- Ling, H.I., Yue, D., Kaliakin, V.N., and Themelis, N.J. 2002. Anisotropic elastoplastic bounding surface model for cohesive soils. *Journal of Engineering Mechanics*. **128**(7): 748-758. doi:10.1061/(ASCE)0733-9399(2002)128:7(748).
- Liu, H.-Y., Abell, J. A., Diambra, A., and Pisanò, F. 2019. Modelling the cyclic ratcheting of sands through memory-enhanced bounding surface plasticity. *Géotechnique*. **69**(9): 783-800. doi:10.1680/jgeot.17.P.307.
- Pan, Y., and Rotta Loria, A. F. 2024. SANISAND-MS-T: Simple ANIsotropic SAND model with memory surface for temperature effects. *Computers and Geotechnics*. **170**: 106303. doi:10.1016/j.compgeo.2024.106303.
- Pestana, J.M., and Whittle, A.J. 1999. Formulation of a unified constitutive model for clays and sands. *International Journal for Numerical and Analytical Methods in Geomechanics*. **23**(12): 1215-1243. doi:10.1002/(SICI)1096-9853(199910)23:12<1215::AID-NAG29>3.0.CO;2-F.
- Poorooshasb, H. B., Holubec, I., and Sherbourne, A. N. 1966. Yielding and Flow of Sand in Triaxial Compression: Part I. *Canadian Geotechnical Journal*. **3**(4): 179-190. doi:10.1139/t66-023.
- Poorooshasb, H. B., Holubec, I., and Sherbourne, A. N. 1967. Yielding and Flow of Sand in Triaxial Compression: Parts II and III. *Canadian Geotechnical Journal*. **4**(4): 375-397. doi:10.1139/t67-066.

- Roscoe, K. H., Schofield, A. N., and Thurairajah, A. 1963. Yielding of clays in state wetter than critical. *Géotechnique*, **13**(3): 211-240. doi:724 .org/10.1680/geot.1963.13.3.211.
- Roscoe, K.H., and Burland, J.B. 1968. On the generalized stress-strain behaviour of ‘wet’ clay. *Engineering Plasticity*. Cambridge, UK: Cambridge University Press, pp. 553-609.
- Sheng, D., Sloan, S.W., and Yu, H.S. 2000. Aspects of finite element implementation of critical state models. *Computational Mechanics*. **26**: 185-196.
doi:10.1007/s004660000166.
- Taiebat, M., and Dafalias, Y. F. 2008. SANISAND: Simple anisotropic sand plasticity model. *International Journal for Numerical and Analytical Methods in Geomechanics*. **32**(8): 915-948. doi:10.1002/nag.651.
- Wheeler, S.J., Näätänen, A., Karstunen, M., and Lojander, M. 2003. An anisotropic elastoplastic model for soft clays. *Canadian Geotechnical Journal*. **40**(2): 403-418.
doi:10.1139/t02-119.
- Yang, J., and Li, X. S. 2004. State-dependent strength of sands from the perspective of unified modeling. *Journal of Geotechnical & Geoenvironmental Engineering*. **130**(2): 186-198. doi:10.1061/(ASCE)1090-0241(2004)130:2(186).
- Yao, Y.-P., Sun, D.-A., and Luo, T. 2004. A critical state model for sands dependent on stress and density. *International Journal for Numerical and Analytical Methods in Geomechanics*. **28**: 323-337. doi:10.1002/nag.340.
- Yao, Y.-P., Hou, W., and Zhou, A.-N. 2009. UH model: three-dimensional unified hardening model for overconsolidated clays. *Géotechnique*. **59**(5): 451-469.
doi:10.1680/geot.2007.00029.
- Yao, Y.-P., Qu S., Yin Z.-Y., and Zhu E.-Y. 2016. SSUH model: A small-strain extension of the unified hardening model. *Science China Technological Sciences*. **59**(2): 225-240.
doi:10.1007/s11431-015-5914-0.

- Yao, Y.-P., Liu, L., Luo, T., Tian, Y., and Zhang, J.-M. 2019. Unified hardening (UH) model for clays and sands. *Computers and Geotechnics*. **110**: 326-343.
doi:10.1139/cgj-2024-0337.
- Yasufuku, N., Murata, H., and Hyodo, M. 1991. Yield characteristics of anisotropically consolidated sand under low and high stresses. *Soils and Foundations*. **31**(1): 95-109.
doi:10.3208/sandf1972.31.95.
- Yin, Z.-Y., and Chang, C.S. 2009. Microstructural modelling of stress-dependent behaviour of clay. *International Journal of Solids and Structures* **46**: 1373-1388.
doi:10.1016/j.ijsolstr.2008.11.006.
- Yin, Z.-Y., Hicher, P.-Y., Dano, C., and Jin, Y.-F. 2016. Modeling Mechanical Behavior of Very Coarse Granular Materials. *Journal of Engineering Mechanics*. **143**(1): C4016006.
doi:10.1061/(ASCE)EM.1943-7889.0001059.
- Yin, Z.-Y., and Li, J. 2025. A general anisotropic yield function for K_0 -consolidated clays. *Canadian Geotechnical Journal*. **62**. doi:10.1139/cgj-2024-0337.
- Yu, H.-S. 1998. CASM: A Unified State Parameter Model for Clay and Sand. *International Journal for Numerical and Analytical Methods in Geomechanics*. **22**(8): 621-653.
doi:10.1002/(SICI)1096-9853(199808)22:8<621::AID-NAG937>3.0.CO;2-8.
- Zhang, F., Ye, B., Noda, T., Nakano, M., and Nakai, K. 2007. Explanation of cyclic mobility of soils: Approach by stress-induced anisotropy. *Soils and Foundations*. **47**(4): 635-648.
doi:10.3208/sandf.47.635.
- Zhang, F., Ye, B., and Ye, G. 2011. Unified description of sand behavior. *Frontiers of Architecture and Civil Engineering in China*, **5**(2): 121-150.
doi:10.1007/s11709-011-0104-z